

Search for $e^+e^- \rightarrow K_S^0 K_S^0 h_c$

The BESIII Collaboration



E-mail: besiii-publications@ihep.ac.cn

ABSTRACT: Using e^+e^- collision data at 13 center-of-mass energies ranging from 4.600 to 4.950 GeV collected with the BESIII detector, we search for the unmeasured $e^+e^- \rightarrow K_S^0 K_S^0 h_c$ process. No significant signal is observed, and the upper limits of the Born cross sections at each center-of-mass energy are presented.

KEYWORDS: e^+e^- collision, Exotic hadron, Quarkonium

ARXIV EPRINT:

Contents

1	Introduction	1
2	BESIII detector and data samples	2
3	Event selection	3
4	Cross section	5
5	Systematic uncertainty	7
6	Summary	9
7	Appendix	10

1 Introduction

Over the last two decades, the discovery of numerous charmonium-like states has significantly expanded our understanding of charmonium spectroscopy. One of the prominent topics in this field is the so-called “ Y -puzzle”, which involves a series of vector states ($J^{PC} = 1^{--}$) collectively referred to as Y states. Above the $D\bar{D}$ threshold, along with the well-established vector charmonium states, several Y states, such as the $Y(4260)$ and $Y(4660)$ [1–3], have been observed. These Y states cannot be easily classified as conventional charmonium states and are thus considered potential candidates for hadrons with exotic internal structures. Hypotheses for their composition include hybrid [4–6], tetraquark [7], molecule [8–10], hadrocharmonium states [11, 12], or kinematically induced peaks [13].

Recently, the BESIII collaboration studied the processes $e^+e^- \rightarrow K^+K^-J/\psi$ [14, 15] and $e^+e^- \rightarrow K_S^0K_S^0J/\psi$ [16]. The cross section line shapes revealed two structures, referred to as $Y(4500)$ and $Y(4710)$, around 4.5 and 4.7 GeV, respectively. Furthermore, in the process $e^+e^- \rightarrow D_s^{*+}D_s^{*-}$, a structure near 4.75 GeV was found as necessary to describe the cross section line shape [17]. These structures are observed in final states containing $s\bar{s}c\bar{c}$ quarks. Studying these Y states across various processes is crucial for advancing our understanding of their nature. The decay of conventional vector charmonium states into h_c is expected to be suppressed due to heavy-quark spin symmetry [18]; thus, searches for Y states decaying into h_c could provide valuable insight into their exotic properties.

To date, the process $e^+e^- \rightarrow K\bar{K}h_c$ remains unobserved. This motivated us to try to measure the cross section line shape of $e^+e^- \rightarrow K\bar{K}h_c$ and to search for potential Y states. In this analysis, we present a study of the process $e^+e^- \rightarrow K_S^0K_S^0h_c$ using 13 data samples collected within the energy range from 4.600 to 4.950 GeV with the BESIII detector [19] at

the BEPCII collider [20]. The study of $e^+e^- \rightarrow K^+K^-h_c$ will be presented in a separate paper. The h_c meson is reconstructed via its radiative decay to η_c . A partial reconstruction method, omitting the reconstruction of the η_c meson, is employed to improve the detection statistics for the signal process.

2 BESIII detector and data samples

The BESIII detector [19] records e^+e^- collisions provided by the BEPCII storage ring [20] in the center-of-mass (c.m.) energy range from 1.84 to 4.95 GeV, with a peak luminosity of $1.1 \times 10^{33} \text{ cm}^{-2}\text{s}^{-1}$ achieved at $\sqrt{s} = 3.773 \text{ GeV}$. The cylindrical core of the BESIII detector covers 93% of the full solid angle and consists of a helium-based multilayer drift chamber (MDC), a plastic scintillator time-of-flight system (TOF), and a CsI(Tl) electromagnetic calorimeter (EMC), which are all enclosed in a superconducting solenoidal magnet providing a 1.0 T magnetic field. The solenoid is supported by an octagonal flux-return yoke with resistive plate counter muon identification modules interleaved with steel. The charged-particle momentum resolution at 1 GeV/c is 0.5%, and the dE/dx resolution is 6% for electrons from Bhabha scattering. The EMC measures photon energies with a resolution of 2.5% (5%) at 1 GeV in the barrel (end cap) region. The time resolution in the TOF barrel region is 68 ps, while that in the end cap region is 110 ps. The end cap TOF system was upgraded in 2015 using multi-gap resistive plate chamber technology, providing a time resolution of 60 ps [21]. All the data samples, except for the one at 4.6 GeV, benefit from the TOF upgrade.

The data samples used for this analysis were collected at 13 c.m. energies (\sqrt{s}) ranging from 4.600 to 4.950 GeV. The c.m. energies are measured by selecting di-muon or $e^+e^- \rightarrow \Lambda_c\bar{\Lambda}_c$ events [22, 23] with an uncertainty of 0.6 MeV. The total integrated luminosity is 6.4 fb^{-1} with an uncertainty of 1.0%, determined by selecting large angle Bhabha scattering events [23, 24]. The process $e^+e^- \rightarrow K_S^0 K_S^0 J/\psi$ is used as a control sample to determine the mass resolution difference between data and Monte Carlo (MC) sample. Data samples with $4.19 < \sqrt{s} < 4.29 \text{ GeV}$, corresponding to an integrated luminosity of 9.5 fb^{-1} , are used to select the control sample events. The momentum range of K_S^0 in the control sample is similar to that in the signal process in data samples taken at $4.6 \text{ GeV} < \sqrt{s} < 4.95 \text{ GeV}$.

Simulated samples are produced with a GEANT4-based [25] MC package, which includes the geometric description of the BESIII detector and the detector response. The simulation models the beam energy spread and initial state radiation (ISR) in the e^+e^- annihilations with the generator KKMC [26]. All particle decays are modeled with EVTGEN [27] using branching fractions either taken from the Particle Data Group (PDG) [1], when available, or otherwise estimated with LUNDCHARM [28]. Final state radiation from charged final state particles is incorporated using PHOTOS [29].

Inclusive MC samples, which include the production of open-charm mesons, the ISR production of vector charmonium(-like) states, and continuum processes, are used to study the background contributions. A signal MC sample of $e^+e^- \rightarrow K_S^0 K_S^0 h_c$ with h_c and η_c decaying inclusively, is used to determine the detection efficiencies. The potential decay of $Y \rightarrow K_S^0 K_S^0 h_c$ is modeled by assuming a phase space (PHSP) distribution. The cross

section of $e^+e^- \rightarrow K_S^0 K_S^0 h_c$ is assumed to follow the three-body decay phase space factor $PS(\sqrt{s})$. For the dominant decay of h_c , $h_c \rightarrow \gamma\eta_c$, the angular distribution of the $E1$ photon (in the h_c rest frame) is generated as $1 + \cos^2\theta$. A MC sample of $e^+e^- \rightarrow K_S^0 K_S^0 J/\psi$ is simulated with $Y \rightarrow K_S^0 K_S^0 J/\psi$ modeled by PHSP [27]. The cross section line shape from a previous measurement [16] is used as input in the simulation of $e^+e^- \rightarrow K_S^0 K_S^0 J/\psi$ events.

3 Event selection

In this analysis, the signal process $K_S^0 K_S^0 h_c$ is reconstructed by selecting two K_S^0 mesons. Given that the decay channel $h_c \rightarrow \gamma\eta_c$ is dominant, an additional photon is reconstructed to enhance the signal significance. Reconstruction of the η_c meson is not made.

A K_S^0 candidate is reconstructed from two oppositely charged tracks, which are assigned as $\pi^+\pi^-$ without imposing further particle identification criteria. These tracks are constrained to originate from a common vertex and are required to have an invariant mass ($M_{\pi^+\pi^-}$) within $(m_{K_S^0} \pm 6)$ MeV/ c^2 , where $m_{K_S^0}$ is the nominal mass of K_S^0 from PDG [1]. The size of the mass window is determined by performing an optimization based on the Punzi Figure-of-Merit (FoM) [30], defined as $\text{FoM} = \frac{\epsilon}{A/2 + \sqrt{B}}$, where A is set to be 3 as the expected significance, ϵ is the efficiency given by the signal MC sample, and B represents the number of background events estimated by the inclusive MC sample normalized according to the integrated luminosity. The $M_{\pi^+\pi^-}$ distribution and the corresponding mass window are shown in figure 1 (left). Additionally, the decay length of the K_S^0 candidate is required to be greater than twice the vertex resolution away from the interaction point (IP).

A photon candidate is identified using showers in the EMC. The deposited energy of a shower must be more than 25 MeV in the barrel region, where the polar angle θ satisfies $|\cos\theta| < 0.8$, and more than 50 MeV in the end cap region ($0.86 < |\cos\theta| < 0.92$). To suppress electronic noise and showers unrelated to the event, the difference between the EMC time and the event start time is required to be within [0, 700] ns. Each signal candidate event is required to contain at least one photon.

After the selections described above, each signal candidate event must contain at least one $K_S^0 K_S^0$ pair with four non-overlapping pions. If multiple $K_S^0 K_S^0$ pairs exist in an event, all combinations are retained for further analysis. Each $K_S^0 K_S^0$ combination is then paired with the photons in the event. The photon with the recoil mass of $\gamma K_S^0 K_S^0$ ($M_{\gamma K_S^0 K_S^0}^{\text{rec}}$) closest to the nominal η_c mass (m_{η_c}) is tagged as the $E1$ photon. The $\gamma K_S^0 K_S^0$ combinations are required to satisfy $M_{\gamma K_S^0 K_S^0}^{\text{rec}} \in [2.94, 3.06]$ GeV/ c^2 , a range optimized based on the Punzi FoM [30]. The $M_{\gamma K_S^0 K_S^0}^{\text{rec}}$ distribution and the mass window are shown in figure 1 (right).

The background contribution from multi $K_S^0 K_S^0$ combinations in the signal process is studied using signal MC simulations with a truth match method. This method compares the 3-momentum of the reconstructed charged pion tracks with the truth information. An observable, defined as $\chi_{\text{match}}^2 = \sum_{i=1}^4 (\vec{p}_{\text{rec},i} - \vec{p}_{\text{truth},i})^2$, is employed to indicate the goodness of the truth match, where $\vec{p}_{\text{rec},i}$ represents the 3-momentum of the i -th pion from the K_S^0 decay after reconstruction, and $\vec{p}_{\text{truth},i}$ denotes the 3-momentum of the i -th pion from the K_S^0 decay at the truth level. If there is more than one such combination in an event, the one

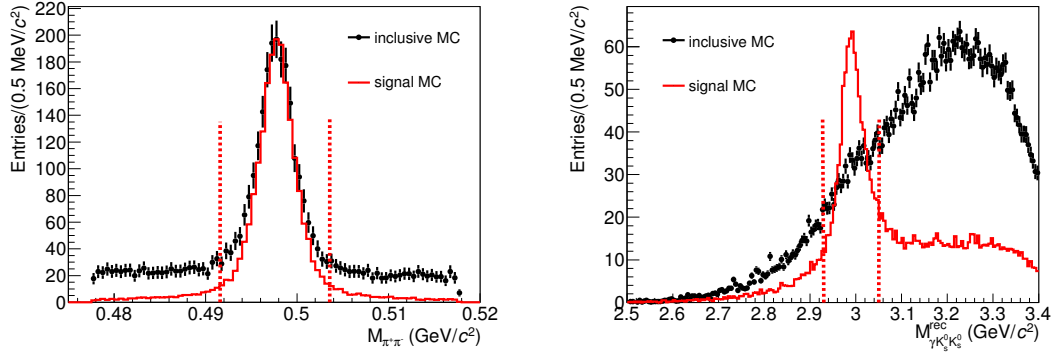


Figure 1. Distributions of $M_{\pi^+\pi^-}$ (left) and $M_{\gamma K_S^0 K_S^0}^{\text{rec}}$ (right). The black dots with error bars are from inclusive MC, the red curves are signal MC, and the vertical dashed lines indicate the optimized selection criteria. h_c decays inclusively in the signal MC sample.

with smallest χ_{match}^2 is selected. The combinations satisfying $\chi_{\text{match}}^2 < 0.05$ are classified as matched. The remaining combinations are identified as combinatorial backgrounds from the signal process. This background contribution is small and smoothly distributed across the $K_S^0 K_S^0$ recoil mass ($M_{K_S^0 K_S^0}^{\text{rec}}$) spectrum. The corresponding distributions from the $h_c \rightarrow \gamma\eta_c$ and $h_c \rightarrow \text{non}-(\gamma\eta_c)$ MC simulations are illustrated in figure 2.

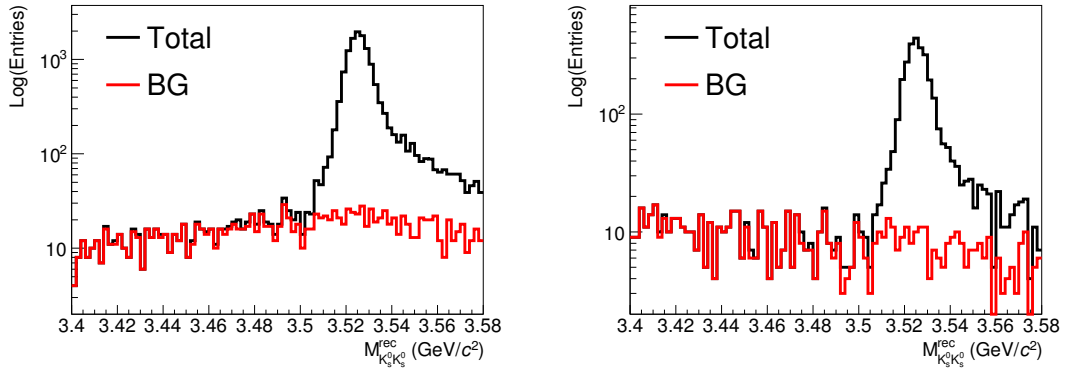


Figure 2. Distributions of $M_{K_S^0 K_S^0}^{\text{rec}}$ from $h_c \rightarrow \gamma\eta_c$ (left) and $h_c \rightarrow \text{non}-(\gamma\eta_c)$ (right). In each panel, the black histogram is the total combinations, the red histogram is the combinatorial background contribution from the signal process.

The same selection criteria are applied to the inclusive MC sample to investigate background contributions from other processes. The background events are found to be dominantly originating from processes with multiple light hadrons in the final state and smoothly distributed in the $M_{K_S^0 K_S^0}^{\text{rec}}$ distribution. The $M_{K_S^0 K_S^0}^{\text{rec}}$ distribution from the inclusive MC sample, normalized according to integrated luminosity, is shown in figure 3 as the brown histogram. The subset of events containing charmonium in the final state is represented by

the gray histogram.

4 Cross section

A fit to the $M_{K_S^0 K_S^0}^{\text{rec}}$ distribution is performed using an unbinned maximum likelihood method to determine the number of $e^+e^- \rightarrow K_S^0 K_S^0 h_c$ signal events. The signal contribution is described by the signal MC shape, convoluted with a Gaussian function to account for the resolution differences between the MC sample and the data. The signal MC shape is parameterized as a sum of four Gaussian functions, with parameters fixed to those determined from the signal MC sample. The parameters of the convoluted Gaussian function, δ_{mean} and δ_σ , are derived from the control sample $e^+e^- \rightarrow K_S^0 K_S^0 J/\psi$ [16]. The selection criteria for the $K_S^0 K_S^0$ pair in the control sample are identical to those used in the signal process. The resolution differences are determined to be $\delta_{\text{mean}} = (0.19 \pm 0.55)$ MeV and $\delta_\sigma = (-0.01 \pm 1.07)$ MeV.

The background contribution for the $e^+e^- \rightarrow K_S^0 K_S^0 h_c$ process is described with a second-order Chebyshev function. The fit results for the $M_{K_S^0 K_S^0}^{\text{rec}}$ distribution from the signal MC and data at $\sqrt{s} = 4.750$ GeV are shown in figure 3. The bottom panels display the distributions of $\chi = \frac{N_{\text{data}} - N_{\text{fit}}}{\delta_{\text{data}}}$, where N_{data} , N_{fit} , and δ_{data} represent the number of events from the data sample, the total fit curve, and the statistical uncertainty of the data, respectively. Fit results for the other data samples are presented in the appendix.

The signal significance for each data sample is evaluated by comparing the difference of $(-\ln L)$ with and without the signal component, where L denotes the likelihood value. The significance is found to be less than 2σ for each data sample, and is not calculated if the nominal signal yield is negative. The upper limit (U.L.) on the number of signal events is determined at the 90% confident level (C.L.) through a likelihood scan. The distribution of L/L_0 as a function of N_{sig} for the $\sqrt{s} = 4.750$ GeV data is shown in figure 4, where L and L_0 are the likelihood values for each N_{sig} and the maximum likelihood value, respectively. The upper limit is determined from $\int_0^{N_{\text{sig}}^{\text{U.L.}}} (L/L_0) dx / \int_0^\infty (L/L_0) dx = 0.9$.

The Born cross section σ_{Born} is calculated using the formula:

$$\sigma_{\text{Born}} = \frac{N_{\text{sig}}}{\epsilon \mathcal{L} (1 + \delta) \delta_{\text{VP}} \mathcal{B}^2(K_S^0 \rightarrow \pi^+ \pi^-)}, \quad (4.1)$$

where ϵ , \mathcal{L} , $(1 + \delta)$, δ_{VP} , and $\mathcal{B}(K_S^0 \rightarrow \pi^+ \pi^-)$ represent the detection efficiency, the integrated luminosity, the ISR correction factor, the vacuum polarization (VP) correction factor [31], and the branching fraction of $K_S^0 \rightarrow \pi^+ \pi^-$, respectively. The upper limit of σ_{Born} is similarly determined by substituting N_{sig} with its upper limit $N_{\text{sig}}^{\text{U.L.}}$. The numerical results for each data sample are listed in table 1 and shown in figure 5. In the table, the second error of σ_{Born} represents the systematic uncertainty, $N_{\text{sig}}^{\text{U.L.,nom}}$ is the nominal upper limit of the signal yields, and $\sigma_{\text{Born}}^{\text{U.L.,sys}}$ reflects the most conservative result incorporating systematic uncertainties that will be discussed in the next section.

To better understand the nature of Y states above 4.6 GeV, we calculate the ratio $R = \frac{\sigma(e^+e^- \rightarrow K_S^0 K_S^0 h_c)}{\sigma(e^+e^- \rightarrow K_S^0 K_S^0 J/\psi)}$. The values of $\sigma(e^+e^- \rightarrow K_S^0 K_S^0 J/\psi)$ are taken from Ref. [14–16]. The results for $\sigma(e^+e^- \rightarrow K_S^0 K_S^0 J/\psi)$ and $\sigma(e^+e^- \rightarrow K^+ K^- J/\psi)$ are combined

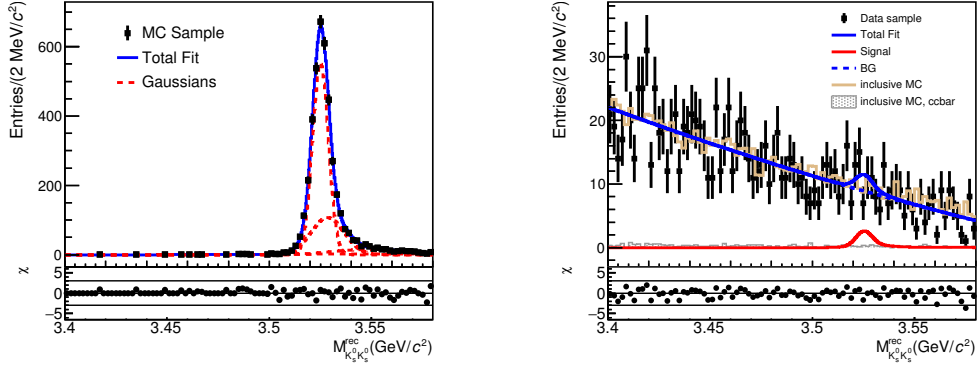


Figure 3. The fit to the $M_{K_S^0 K_S^0}^{\text{rec}}$ distribution from $e^+e^- \rightarrow K_S^0 K_S^0 h_c$ process at $\sqrt{s} = 4.750$ GeV. The left panel shows the fit to signal MC, where the blue solid line and the red dashed lines represent the total fit curve and the four Gaussian functions, respectively. The right panel shows the fit to data, where the blue solid line is the total fit curve, the blue dashed line is the background contribution, and the red line is the fitted signal contribution. The contribution from the inclusive MC sample is also shown. The brown histogram and the gray filled histogram are the total inclusive MC and the events with charmonium in the final state, respectively. The χ distributions are shown below.

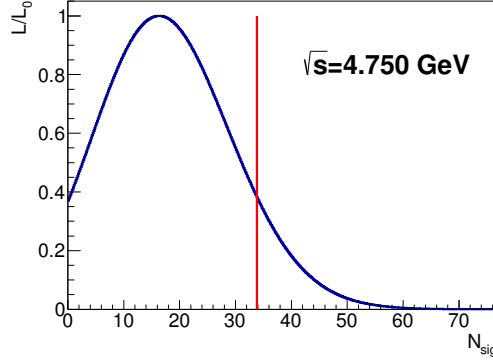


Figure 4. The likelihood scan result at the $\sqrt{s} = 4.750$ GeV data sample. The red vertical line indicates the position of the U.L. at the 90% C.L.

assuming isospin symmetry. Since all three measurements are dominated by the statistical uncertainty, the quadratic sum of the statistical and systematic uncertainties of each process is used. The results for R are presented in figure 6. Fitting the ratio with a constant term, the average ratio is determined to be 0.15 ± 0.22 . The upper limit of the cross section ratio is calculated by replacing $\sigma(e^+e^- \rightarrow K_S^0 K_S^0 h_c)$ with $\sigma^{\text{U.L.,sys}}(e^+e^- \rightarrow K_S^0 K_S^0 h_c)$, determined with the uncertainties of the $\sigma(e^+e^- \rightarrow K_S^0 K_S^0 J/\psi)$ included as one source of systematic uncertainty.

Table 1. The numerical results of the Born cross section for each data sample. The numbers in brackets are upper limits at the 90% C.L. Shown are also the c.m. energies \sqrt{s} , the integrated luminosity \mathcal{L} , the number of signal events (the upper limits) N_{sig} ($N_{\text{sig}}^{\text{U.L.,nom}}$), the efficiency ϵ , the VP correction factor δ_{VP} , the ISR correction factor $(1 + \delta)$, the significance at each data sample and the ratio $R = \frac{\sigma(e^+e^- \rightarrow K_S^0 K_S^0 h_c)}{\sigma(e^+e^- \rightarrow K_S^0 K_S^0 J/\psi)}$.

\sqrt{s}	\mathcal{L} (pb $^{-1}$)	N_{sig} ($N_{\text{sig}}^{\text{U.L.,nom}}$)	ϵ (%)	δ_{VP}	$1 + \delta$	Significance	σ_{Born} ($\sigma_{\text{Born}}^{\text{U.L.,sys}}$) (pb)	R ($R^{\text{U.L.}}$)
4.600	587	$10.3^{+7.0}_{-6.3}$ (< 20.4)	8.4	1.055	0.720	1.7σ	$0.58^{+0.40}_{-0.36} \pm 0.07$ (< 1.27)	$0.7^{+0.5}_{-0.4}$ (< 1.6)
4.612	104	$-3.1^{+2.8}_{-1.8}$ (< 4.8)	7.6	1.055	0.731	–	$-1.07^{+0.96}_{-0.65} \pm 0.14$ (< 1.91)	$-3.3^{+3.9}_{-2.5}$ (< 6.5)
4.628	522	$-9.4^{+6.6}_{-5.8}$ (< 8.3)	7.9	1.054	0.741	–	$-0.61^{+0.44}_{-0.38} \pm 0.08$ (< 0.63)	$-1.1^{+0.8}_{-0.7}$ (< 1.2)
4.641	552	$-12.8^{+7.8}_{-7.0}$ (< 8.8)	8.0	1.054	0.745	–	$-0.78^{+0.48}_{-0.43} \pm 0.08$ (< 0.62)	$-1.5^{+1.0}_{-0.9}$ (< 1.3)
4.661	529	$9.8^{+9.7}_{-8.9}$ (< 23.8)	8.3	1.054	0.756	1.1σ	$0.59^{+0.58}_{-0.54} \pm 0.05$ (< 1.56)	$1.0^{+1.0}_{-0.9}$ (< 3.0)
4.682	1667	$-9.3^{+18.2}_{-17.3}$ (< 25.9)	8.6	1.054	0.764	–	$-0.17^{+0.33}_{-0.32} \pm 0.01$ (< 0.71)	$-0.2^{+0.5}_{-0.4}$ (< 1.0)
4.699	536	$4.3^{+11.8}_{-11.0}$ (< 23.0)	8.4	1.055	0.769	0.4σ	$0.25^{+0.68}_{-0.63} \pm 0.02$ (< 1.47)	$0.3^{+0.8}_{-0.7}$ (< 1.8)
4.740	165	$0.4^{+7.4}_{-6.6}$ (< 13.4)	9.1	1.055	0.781	0.1σ	$0.07^{+1.26}_{-1.12} \pm 0.03$ (< 2.42)	$0.2^{+1.4}_{-1.2}$ (< 2.8)
4.750	367	$16.4^{+12.5}_{-11.7}$ (< 33.8)	9.2	1.055	0.782	1.4σ	$1.22^{+0.94}_{-0.88} \pm 0.09$ (< 2.69)	$1.1^{+0.9}_{-0.8}$ (< 2.7)
4.781	511	$-0.3^{+14.6}_{-13.7}$ (< 24.7)	9.4	1.055	0.788	–	$-0.02^{+0.76}_{-0.72} \pm 0.01$ (< 1.61)	$0^{+0.7}_{-0.6}$ (< 1.5)
4.843	525	$2.1^{+15.5}_{-14.7}$ (< 27.7)	9.3	1.056	0.802	0.1σ	$0.11^{+0.78}_{-0.74} \pm 0.02$ (< 1.48)	$0.2^{+1.1}_{-1.1}$ (< 2.3)
4.918	208	$11.7^{+11.2}_{-10.5}$ (< 27.9)	9.7	1.056	0.814	1.1σ	$1.41^{+1.37}_{-1.28} \pm 0.17$ (< 3.60)	$2.2^{+2.3}_{-2.1}$ (< 6.6)
4.951	159	$-1.6^{+9.5}_{-8.6}$ (< 15.6)	9.6	1.056	0.818	–	$-0.26^{+1.49}_{-1.36} \pm 0.02$ (< 3.07)	$-0.6^{+3.3}_{-3.0}$ (< 7.6)

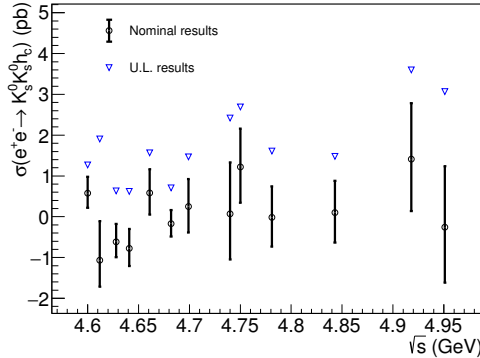


Figure 5. The nominal result (dots with error bars) and the U.L. (triangular points) of the Born cross section of $e^+e^- \rightarrow K_S^0 K_S^0 h_c$.

5 Systematic uncertainty

The uncertainties in the measured Born cross sections arise from various sources, which contribute either as multiplicative or additive terms. The multiplicative terms include integrated luminosity, input branching fractions, and detection efficiency. Additive terms stem from the determination of N_{sig} and the line shape of the cross section. The uncertainties are combined in quadrature to calculate the total systematic uncertainty, assuming they are independent. For the upper limit, the uncertainty from multiplicative terms, summarized in table 2, is incorporated by convoluting a Gaussian function into the likelihood distribu-

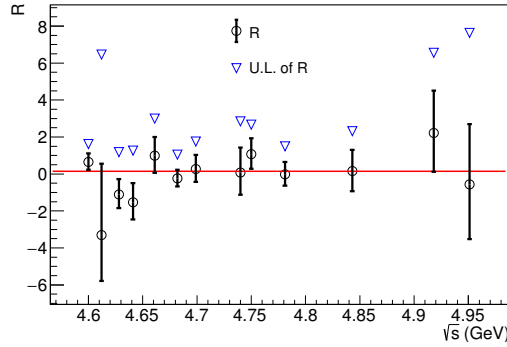


Figure 6. The ratio $R = \frac{\sigma(e^+e^- \rightarrow K_S^0 K_S^0 h_c)}{\sigma(e^+e^- \rightarrow K_S^0 K_S^0 J/\psi)}$ and its upper limit. The red line indicates the average value.

tion. The likelihood distribution is derived from the most conservative result based on the additive terms.

Table 2. Summary of multiplicative systematic uncertainties.

Source	Uncertainty (%)
Luminosity	1.0
$\mathcal{B}(h_c \rightarrow \gamma\eta_c)$	4.3
Photon reconstruction	1.0
K_S^0 reconstruction	2.6 – 8.8
η_c mass window	1.0
Total	5.4 – 10.0

The integrated luminosity is measured by selecting Bhabha scattering events, with an associated uncertainty of 1.0% [23, 24]. Since the processes $h_c \rightarrow \gamma\eta_c$ and $h_c \rightarrow \text{non}-(\gamma\eta_c)$ are both considered as signal, the uncertainty from $\mathcal{B}(h_c \rightarrow \gamma\eta_c)$, for which the best measurement yields $\mathcal{B}(h_c \rightarrow \gamma\eta_c) = (57.66_{-3.50}^{+3.62} \pm 0.58)\%$ [32], is estimated by modifying the value by $\pm 1\sigma$. The resulting change in the detection efficiency ϵ of 4.3% is taken as the systematic uncertainty.

The uncertainty from photon reconstruction is studied using control samples of $J/\psi \rightarrow \rho\pi^0$ and $e^+e^- \rightarrow \gamma\gamma$, and is determined to be 1% per photon [33]. The uncertainty from K_S^0 reconstruction is assessed by selecting the decay $J/\psi \rightarrow K^{*\pm}\bar{K}^\mp$ as a control sample. The reconstruction efficiency difference between data and MC sample as a function of the momentum of K_S^0 ($p_{K_S^0}$) is provided. By weighing the efficiency difference according to $p_{K_S^0}$ in the signal process across various data samples, the systematic uncertainty from K_S^0 is estimated to range from 4.4% to 1.3% per K_S^0 for \sqrt{s} ranging from 4.600 GeV to 4.950 GeV. Uncertainties from the parameters of η_c in the MC sample are estimated by varying the mass and width separately by $\pm 1\sigma$, resulting in an uncertainty of 0.5%, where σ values are

cited from PDG [1]. The uncertainty from the line shape of η_c [34] used in MC samples is estimated by incorporating the missing term (E_γ^3), resulting in a difference in detection efficiencies of 0.8%. Consequently, the total uncertainty from the η_c mass window is 1%.

In the fit to the $M_{K_S^0 K_S^0}^{\text{rec}}$ distribution, the uncertainty due to the resolution difference between data and MC sample is estimated by generating toy MC samples with parameters modified by 0 or $\pm 1\sigma$. This results in one set of nominal shape MC samples and eight sets for the modified shapes. The toy MC samples are then fitted using the nominal line shape. The systematic uncertainty is determined by comparing the fit results obtained from toy MC samples based on the nominal and modified shapes, which is found to range within $\delta(N_{\text{sig}}) = (0.0, 0.5)$ for different data samples. For the upper limit, the uncertainty is estimated by repeating the scan with the modified shape. The uncertainty from the fit range is assessed following the discussion in [35, 36]. The lower and upper boundaries of the fit range are modified separately by $\pm 5 \text{ MeV}/c^2$ and $\pm 10 \text{ MeV}/c^2$. The study indicates that the effect of the fit range is negligible. The systematic uncertainty arising from the background model is assessed by repeating the fit with the second-order Chebyshev function modified to a third-order Chebyshev function. The change in the value of $(-\ln L)$, which measures the improvement, is found to be negligible. The likelihood scan is repeated with the modified background shape, and the largest U.L. is taken as a conservative estimation.

The input cross section line shape affects not only the ISR correction factor $(1 + \delta)$ and the detection efficiency but also the signal shape. In the nominal result, the cross section is assumed to follow $PS(\sqrt{s})$. We then modify it to reflect the measured cross section line shape of the $e^+e^- \rightarrow K_S^0 K_S^0 J/\psi$ process [16] and take the difference in the fit to estimate the effect. This uncertainty on the cross section is determined to range within $\delta(\sigma) = (0.01, 0.15) \text{ pb}$ for the data samples.

6 Summary

In summary, we searched for the process $e^+e^- \rightarrow K_S^0 K_S^0 h_c$ using 13 data samples collected by the BESIII detector at \sqrt{s} ranging from 4.600 GeV to 4.950 GeV. The significance of the signal process is found to be below 2σ for each c.m. energy. The upper limits of the cross section for each data sample are determined at the 90% C.L. based on the current statistics. There appears to be a slight enhancement of the cross section around 4.75 GeV, but no definitive conclusions can be made regarding whether $Y(4710)$ or $Y(4750)$ decay into $K_S^0 K_S^0 h_c$. The ratio $R = \frac{\sigma(e^+e^- \rightarrow K_S^0 K_S^0 h_c)}{\sigma(e^+e^- \rightarrow K_S^0 K_S^0 J/\psi)}$, calculated by combining the measurements of $\sigma(e^+e^- \rightarrow K_S^0 K_S^0 J/\psi)$ and $\sigma(e^+e^- \rightarrow K^+ K^- J/\psi)$, yields an average value of 0.15 ± 0.22 . This ratio suggests that the decay of the Y states into h_c is substantially smaller than into J/ψ , which differs from the ratio $\frac{\sigma(e^+e^- \rightarrow \pi^+ \pi^- h_c)}{\sigma(e^+e^- \rightarrow \pi^+ \pi^- J/\psi)}$ in the range $4.2 < \sqrt{s} < 4.4 \text{ GeV}$. The planned upgrade of the BEPCII [37] and the anticipated increase in statistical data in the near future will enable more precise results for understanding the $Y(4710)$ and $Y(4750)$ states.

Acknowledgments

The BESIII Collaboration thanks the staff of BEPCII and the IHEP computing center for their strong support. This work is supported in part by National Key R&D Program of China under Contracts Nos. 2020YFA0406300, 2020YFA0406400, 2023YFA1606000; National Natural Science Foundation of China (NSFC) under Contracts Nos. 11635010, 11735014, 11935015, 11935016, 11935018, 12025502, 12035009, 12035013, 12061131003, 12192260, 12192261, 12192262, 12192263, 12192264, 12192265, 12221005, 12225509, 12235017, 12361141819, 12375070; the Chinese Academy of Sciences (CAS) Large-Scale Scientific Facility Program; the CAS Center for Excellence in Particle Physics (CCEPP); Joint Large-Scale Scientific Facility Funds of the NSFC and CAS under Contract No. U2032108; Shanghai Leading Talent Program of Eastern Talent Plan under Contract No. J LH5913002; 100 Talents Program of CAS; The Institute of Nuclear and Particle Physics (INPAC) and Shanghai Key Laboratory for Particle Physics and Cosmology; German Research Foundation DFG under Contracts Nos. FOR5327, GRK 2149; Istituto Nazionale di Fisica Nucleare, Italy; Knut and Alice Wallenberg Foundation under Contracts Nos. 2021.0174, 2021.0299; Ministry of Development of Turkey under Contract No. DPT2006K-120470; National Research Foundation of Korea under Contract No. NRF-2022R1A2C1092335; National Science and Technology fund of Mongolia; National Science Research and Innovation Fund (NSRF) via the Program Management Unit for Human Resources & Institutional Development, Research and Innovation of Thailand under Contracts Nos. B16F640076, B50G670107; Polish National Science Centre under Contract No. 2019/35/O/ST2/02907; Swedish Research Council under Contract No. 2019.04595; The Swedish Foundation for International Cooperation in Research and Higher Education under Contract No. CH2018-7756; U. S. Department of Energy under Contract No. DE-FG02-05ER41374

7 Appendix

The following plots display the fit results for each data sample. Each figure consists of three panels: the left panel shows the fit to the MC sample, the middle panel shows the fit to the data, and the right panel displays the likelihood scan. In the left panel, the black dots with error bars, the blue histogram, and the red dashed histograms represent the MC sample, the total fit, and the signal modeled by Gaussian functions, respectively. In the middle panel, the black dots with error bars, the blue histogram, the blue dashed histogram, and the red histogram represent the data sample, the total fit, the background contribution, and the signal. The χ distribution is presented in the bottom panels for the fit to the MC and data samples. The red vertical line in the right panel represents the upper limit at 90% C.L.

References

- [1] Particle Data Group, *Review of Particle Physics*, [PTEP **2022**, 083C01 \(2022\)](#).
- [2] BaBar Collaboration, *Observation of a broad structure in the $\pi^+\pi^-J/\psi$ mass spectrum around $4.26\text{ GeV}/c^2$* , [Phys. Rev. Lett. **95**, 142001 \(2005\)](#).

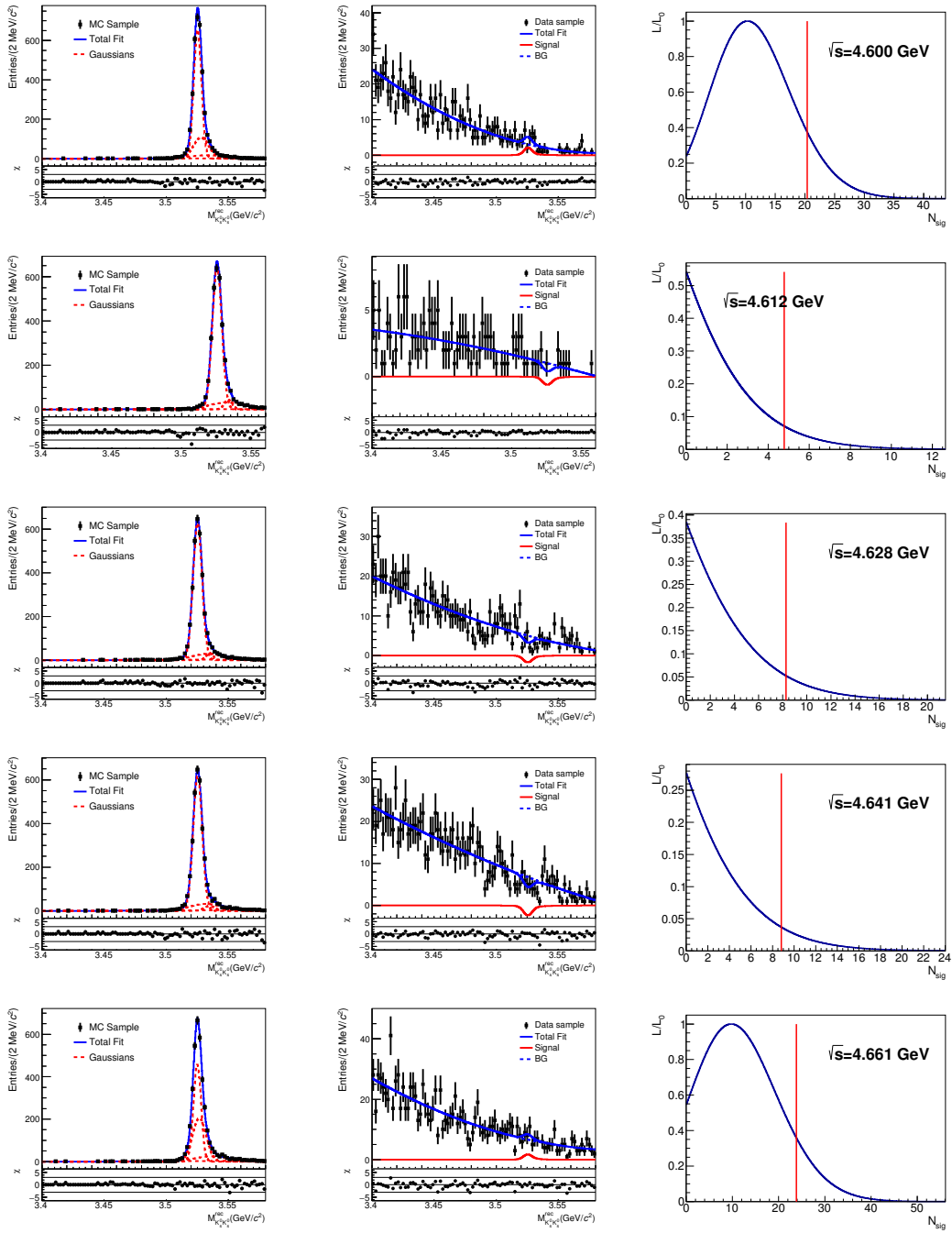


Figure 7. Fit and scan results at $\sqrt{s} = 4.600 - 4.661$ GeV.

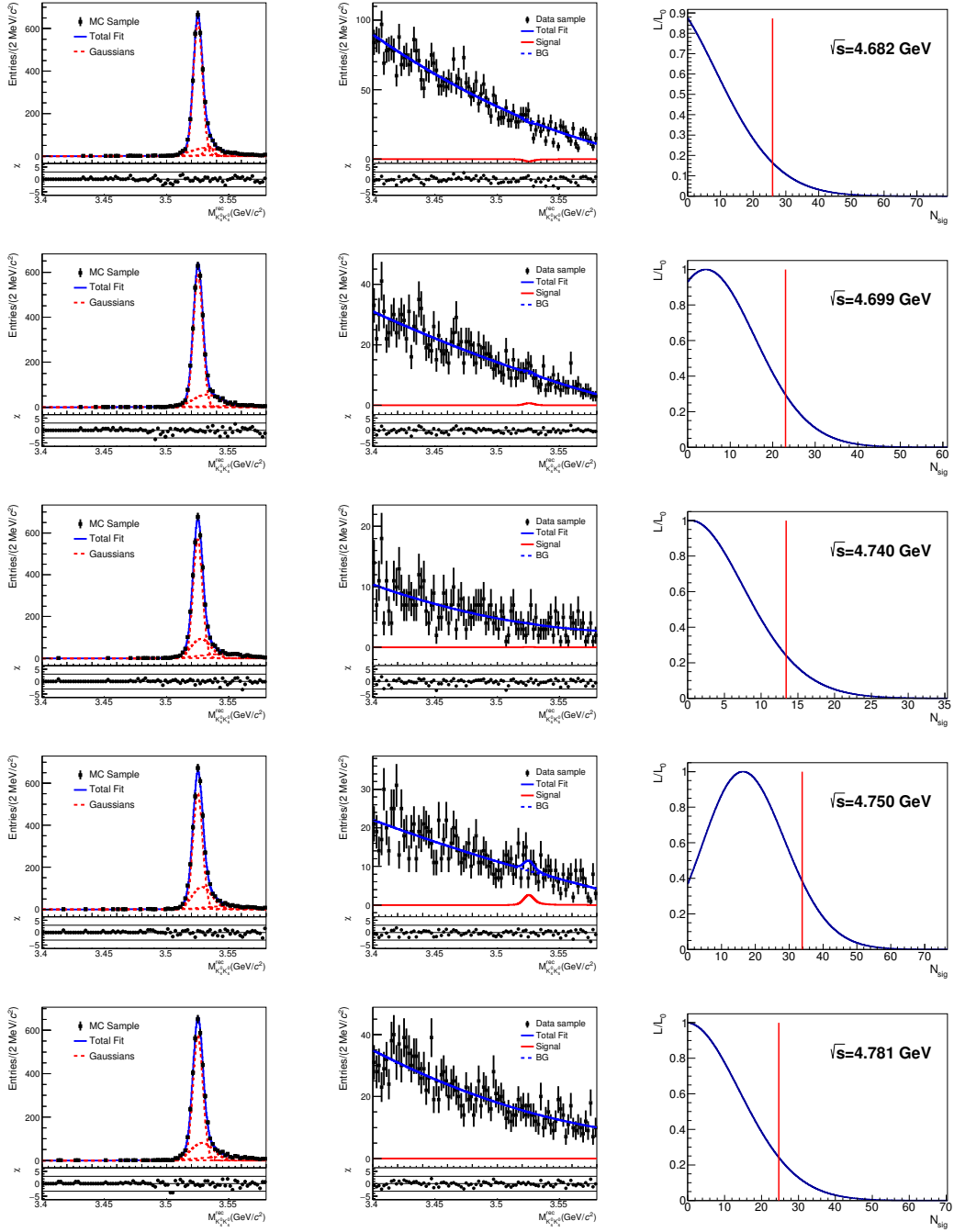


Figure 8. Fit and scan results at $\sqrt{s} = 4.682 - 4.781$ GeV.

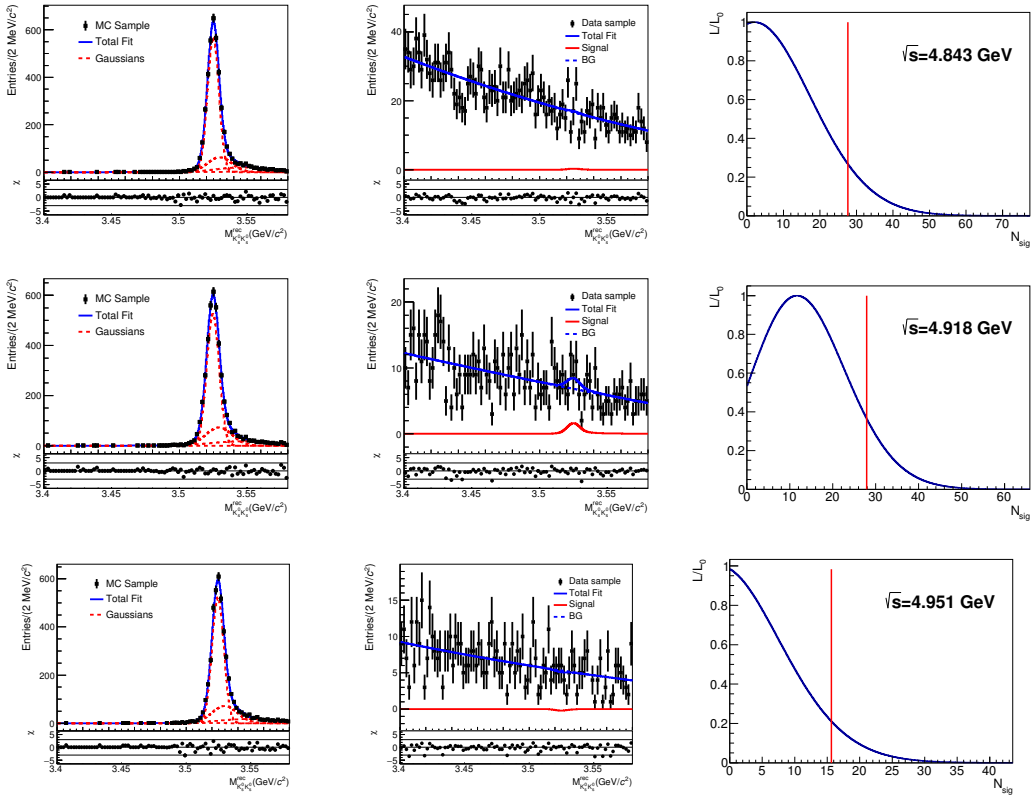


Figure 9. Fit and scan results at $\sqrt{s} = 4.843 - 4.951$ GeV.

- [3] Belle Collaboration, *Observation of Two Resonant Structures in e^+e^- to $\pi^+\pi^-\psi'$ via Initial State Radiation at Belle*, *Phys. Rev. Lett.* **99**, 142002 (2007).
- [4] S. L. Zhu, *The Possible interpretations of $Y(4260)$* , *Phys. Lett. B* **625**, 212 (2005).
- [5] F. E. Close and P. R. Page, *Gluonic charmonium resonances at BaBar and BELLE?*, *Phys. Lett. B* **628**, 215-222 (2005).
- [6] E. Kou and O. Pene, *Suppressed decay into open charm for the $Y(4260)$ being an hybrid*, *Phys. Lett. B* **631**, 164-169 (2005).
- [7] L. Maiani, F. Piccinini, A. D. Polosa and V. Riquer, *The $Z(4430)$ and a New Paradigm for Spin Interactions in Tetraquarks*, *Phys. Rev. D* **89**, 114010 (2014).
- [8] M. Cleven, Q. Wang, F. K. Guo, C. Hanhart, U. G. Meißner and Q. Zhao, *$Y(4260)$ as the first S -wave open charm vector molecular state?*, *Phys. Rev. D* **90**, 074039 (2014).
- [9] G. J. Ding, *Are $Y(4260)$ and Z_2^+ are D_1D or D_0D^* Hadronic Molecules?*, *Phys. Rev. D* **79**, 014001 (2009).
- [10] Q. Wang, C. Hanhart and Q. Zhao, *Decoding the riddle of $Y(4260)$ and $Z_c(3900)$* , *Phys. Rev. Lett.* **111**, 132003 (2013).
- [11] S. Dubynskiy and M. B. Voloshin, *Hadro-Charmonium*, *Phys. Lett. B* **666**, 344-346 (2008).

- [12] X. Li and M. B. Voloshin, *Y(4260) and Y(4360) as mixed hadrocharmonium*, *Mod. Phys. Lett. A* **29**, 1450060 (2014).
- [13] D. Y. Chen, X. Liu and T. Matsuki, *Interference effect as resonance killer of newly observed charmoniumlike states Y(4320) and Y(4390)*, *Eur. Phys. J. C* **78**, 136 (2018).
- [14] BESIII Collaboration, *Observation of the Y(4230) and a new structure in $e^+e^- \rightarrow K^+K^-J/\psi$* , *Chin. Phys. C* **46**, 111002 (2022).
- [15] BESIII Collaboration, *Observation of a Vector Charmoniumlike State at 4.7 GeV/c² and Search for Z_{cs} in $e^+e^- \rightarrow K^+K^-J/\psi$* , *Phys. Rev. Lett.* **131**, 211902 (2023).
- [16] BESIII Collaboration, *Observation of the Y(4230) and evidence for a new vector charmoniumlike state Y(4710) in $e^+e^- \rightarrow K_S^0 K_S^0 J/\psi$* , *Phys. Rev. D* **107**, 092005 (2023).
- [17] BESIII Collaboration, *Precise Measurement of the $e^+e^- \rightarrow D_s^{*+} D_s^{*-}$ Cross Sections at Center-of-Mass Energies from Threshold to 4.95 GeV*, *Phys. Rev. Lett.* **131**, 151903 (2023).
- [18] R. Oncala and J. Soto, *Heavy Quarkonium Hybrids: Spectrum, Decay and Mixing*, *Phys. Rev. D* **96**, 014004 (2017).
- [19] BESIII Collaboration, *Design and Construction of the BESIII Detector*, *Nucl. Instrum. Meth. A* **614**, 345 (2010).
- [20] C. H. Yu *et al.*, *BEPCII Performance and Beam Dynamics Studies on Luminosity*, Proceedings of IPAC2016, Busan, Korea, 2016.
- [21] X. Li *et al.*, *Study of MRPC technology for BESIII endcap-TOF upgrade*, *Radiat. Detect. Technol. Methods* **1**, 13 (2017); Y. X. Guo *et al.*, *The study of time calibration for upgraded end cap TOF of BESIII*, *Radiat. Detect. Technol. Methods* **1**, 15 (2017); P. Cao *et al.*, *Design and construction of the new BESIII endcap Time-of-Flight system with MRPC Technology* *Nucl. Instrum. Meth. A* **953**, 163053 (2020).
- [22] BESIII Collaboration, *Measurements of the center-of-mass energies of collisions at BESIII*, *Chin. Phys. C* **45**, 103001 (2021).
- [23] BESIII Collaboration, *Luminosities and energies of e^+e^- collision data taken between 4.61 GeV and 4.95 GeV at BESIII*, *Chin. Phys. C* **46**, 113003 (2022).
- [24] BESIII Collaboration, *Measurement of integrated luminosities at BESIII for data samples at center-of-mass energies between 4.0 and 4.6 GeV*, *Chin. Phys. C* **46**, 113002 (2022).
- [25] GEANT4 Collaboration, *GEANT4: A Simulation toolkit*, *Nucl. Instrum. Meth. A* **506**, 250 (2003).
- [26] S. Jadach, B. F. L. Ward and Z. Was, *Coherent exclusive exponentiation for precision Monte Carlo calculations*, *Phys. Rev. D* **63**, 113009 (2001); *The Precision Monte Carlo event generator KK for two fermion final states in e^+e^- collisions*, *Comput. Phys. Commun.* **130**, 260 (2000).
- [27] D. J. Lange, *The EvtGen particle decay simulation package*, *Nucl. Instrum. Meth. A* **462**, 152 (2001); R. G. Ping, *Event generators at BESIII*, *Chin. Phys. C* **32**, 599 (2008).
- [28] J. C. Chen, G. S. Huang, X. R. Qi, D. H. Zhang and Y. S. Zhu, *Event generator for J/ψ and ψ(2S) decay*, *Phys. Rev. D* **62**, 034003 (2000); R. L. Yang, R. G. Ping and H. Chen, *Tuning and Validation of the Lundcharm Model with J/ψ Decays*, *Chin. Phys. Lett.* **31**, 061301 (2014).

- [29] E. Richter-Was, *QED bremsstrahlung in semileptonic B and leptonic tau decays*, *Phys. Lett. B* **303**, 163 (1993).
- [30] G. Punzi, *Sensitivity of searches for new signals and its optimization*, *eConf C030908*, MODT002 (2003).
- [31] Working Group on Radiative Corrections and Monte Carlo Generators for Low Energies, *Quest for precision in hadronic cross sections at low energy: Monte Carlo tools vs. experimental data*, *Eur. Phys. J. C* **66**, 585-686 (2010).
- [32] BESIII Collaboration, *Study of the $h_c(1^1P_1)$ meson via $\psi(2S) \rightarrow \pi^0 h_c$ decays at BESIII*, *Phys. Rev. D* **106**, 072007 (2022).
- [33] BESIII Collaboration, *Measurement of the branching fraction of $J/\psi \rightarrow \omega \eta' \pi^+ \pi^-$ and search for $J/\psi \rightarrow \omega X(1835)$, $X(1835) \rightarrow \eta' \pi^+ \pi^-$ decay*, *Phys. Rev. D* **99**, 071101 (2019).
- [34] V. V. Anashin, *et al.* *Measurement of $\mathcal{B}(J/\psi \rightarrow \eta_c \gamma)$ at KEDR*, *Int. J. Mod. Phys. Conf. Ser.* **02**, 188-192 (2011).
- [35] R. Barlow, *Systematic errors: Facts and fictions*, [arXiv:hep-ex/0207026](https://arxiv.org/abs/hep-ex/0207026) [hep-ex].
- [36] R. Wanke, *Data Analysis in High Energy Physics: A Practical Guide to Statistical Methods*, edited by O. Behnke, K. Kroninger, G. P. Schott, and T. Schorner-Sadenius (Wiley-VCH Verlag GmbH & Co. KGaA, 2013).
- [37] BESIII Collaboration, *Future Physics Programme of BESIII*, *Chin. Phys. C* **44**, 040001 (2020).

The BESIII collaboration

M. Ablikim¹, M. N. Achasov^{4,c}, P. Adlarson⁷⁶, O. Afedulidis³, X. C. Ai⁸¹, R. Aliberti³⁵,
A. Amoroso^{75A,75C}, Q. An^{72,58,a}, Y. Bai⁵⁷, O. Bakina³⁶, I. Balossino^{29A}, Y. Ban^{46,h}, H.-R. Bao⁶⁴,
V. Batozskaya^{1,44}, K. Begzsuren³², N. Berger³⁵, M. Berlowski⁴⁴, M. Bertani^{28A}, D. Bettoni^{29A},
F. Bianchi^{75A,75C}, E. Bianco^{75A,75C}, A. Bortone^{75A,75C}, I. Boyko³⁶, R. A. Briere⁵,
A. Brueggemann⁶⁹, H. Cai⁷⁷, X. Cai^{1,58}, A. Calcaterra^{28A}, G. F. Cao^{1,64}, N. Cao^{1,64},
S. A. Cetin^{62A}, X. Y. Chai^{46,h}, J. F. Chang^{1,58}, G. R. Che⁴³, Y. Z. Che^{1,58,64}, G. Chelkov^{36,b},
C. Chen⁴³, C. H. Chen⁹, Chao Chen⁵⁵, G. Chen¹, H. S. Chen^{1,64}, H. Y. Chen²⁰,
M. L. Chen^{1,58,64}, S. J. Chen⁴², S. L. Chen⁴⁵, S. M. Chen⁶¹, T. Chen^{1,64}, X. R. Chen^{31,64},
X. T. Chen^{1,64}, Y. B. Chen^{1,58}, Y. Q. Chen³⁴, Z. J. Chen^{25,i}, S. K. Choi¹⁰, G. Cibinetto^{29A},
F. Cossio^{75C}, J. J. Cui⁵⁰, H. L. Dai^{1,58}, J. P. Dai⁷⁹, A. Dbeyssi¹⁸, R. E. de Boer³, D. Dedovich³⁶,
C. Q. Deng⁷³, Z. Y. Deng¹, A. Denig³⁵, I. Denysenko³⁶, M. Destefanis^{75A,75C}, F. De Mori^{75A,75C},
B. Ding^{67,1}, X. X. Ding^{46,h}, Y. Ding³⁴, Y. Ding⁴⁰, J. Dong^{1,58}, L. Y. Dong^{1,64}, M. Y. Dong^{1,58,64},
X. Dong⁷⁷, M. C. Du¹, S. X. Du⁸¹, Y. Y. Duan⁵⁵, Z. H. Duan⁴², P. Egorov^{36,b}, G. F. Fan⁴²,
J. J. Fan¹⁹, Y. H. Fan⁴⁵, J. Fang^{1,58}, J. Fang⁵⁹, S. S. Fang^{1,64}, W. X. Fang¹, Y. Q. Fang^{1,58},
R. Farinelli^{29A}, L. Fava^{75B,75C}, F. Feldbauer³, G. Felici^{28A}, C. Q. Feng^{72,58}, J. H. Feng⁵⁹,
Y. T. Feng^{72,58}, M. Fritsch³, C. D. Fu¹, J. L. Fu⁶⁴, Y. W. Fu^{1,64}, H. Gao⁶⁴, X. B. Gao⁴¹,
Y. N. Gao¹⁹, Y. N. Gao^{46,h}, Yang Gao^{72,58}, S. Garbolino^{75C}, I. Garzia^{29A,29B}, P. T. Ge¹⁹,
Z. W. Ge⁴², C. Geng⁵⁹, E. M. Gersabeck⁶⁸, A. Gilman⁷⁰, K. Goetzen¹³, L. Gong⁴⁰,
W. X. Gong^{1,58}, W. Gradl³⁵, S. Gramigna^{29A,29B}, M. Greco^{75A,75C}, M. H. Gu^{1,58}, Y. T. Gu¹⁵,
C. Y. Guan^{1,64}, A. Q. Guo^{31,64}, L. B. Guo⁴¹, M. J. Guo⁵⁰, R. P. Guo⁴⁹, Y. P. Guo^{12,g},
A. Guskov^{36,b}, J. Gutierrez²⁷, K. L. Han⁶⁴, T. T. Han¹, F. Hanisch³, X. Q. Hao¹⁹, F. A. Harris⁶⁶,
K. K. He⁵⁵, K. L. He^{1,64}, F. H. Heinsius³, C. H. Heinz³⁵, Y. K. Heng^{1,58,64}, C. Herold⁶⁰,
T. Holtmann³, P. C. Hong³⁴, G. Y. Hou^{1,64}, X. T. Hou^{1,64}, Y. R. Hou⁶⁴, Z. L. Hou¹, B. Y. Hu⁵⁹,
H. M. Hu^{1,64}, J. F. Hu^{56,j}, Q. P. Hu^{72,58}, S. L. Hu^{12,g}, T. Hu^{1,58,64}, Y. Hu¹, G. S. Huang^{72,58},
K. X. Huang⁵⁹, L. Q. Huang^{31,64}, P. Huang⁴², X. T. Huang⁵⁰, Y. P. Huang¹, Y. S. Huang⁵⁹,
T. Hussain⁷⁴, F. Hölzken³, N. Hüskens³⁵, N. in der Wiesche⁶⁹, J. Jackson²⁷, S. Janchiv³², Q. Ji¹,
Q. P. Ji¹⁹, W. Ji^{1,64}, X. B. Ji^{1,64}, X. L. Ji^{1,58}, Y. Y. Ji⁵⁰, X. Q. Jia⁵⁰, Z. K. Jia^{72,58}, D. Jiang^{1,64},
H. B. Jiang⁷⁷, P. C. Jiang^{46,h}, S. S. Jiang³⁹, T. J. Jiang¹⁶, X. S. Jiang^{1,58,64}, Y. Jiang⁶⁴,
J. B. Jiao⁵⁰, J. K. Jiao³⁴, Z. Jiao²³, S. Jin⁴², Y. Jin⁶⁷, M. Q. Jing^{1,64}, X. M. Jing⁶⁴,
T. Johansson⁷⁶, S. Kabana³³, N. Kalantar-Nayestanaki⁶⁵, X. L. Kang⁹, X. S. Kang⁴⁰,
M. Kavatsyuk⁶⁵, B. C. Ke⁸¹, V. Khachatryan²⁷, A. Khoukaz⁶⁹, R. Kiuchi¹, O. B. Kolcu^{62A},
B. Kopf³, M. Kuessner³, X. Kui^{1,64}, N. Kumar²⁶, A. Kupsc^{44,76}, W. Kühn³⁷, W. N. Lan¹⁹,
T. T. Lei^{72,58}, Z. H. Lei^{72,58}, M. Lellmann³⁵, T. Lenz³⁵, C. Li⁴⁷, C. Li⁴³, C. H. Li³⁹, Cheng Li^{72,58},
D. M. Li⁸¹, F. Li^{1,58}, G. Li¹, H. B. Li^{1,64}, H. J. Li¹⁹, H. N. Li^{56,j}, Hui Li⁴³, J. R. Li⁶¹, J. S. Li⁵⁹,
K. Li¹, K. L. Li¹⁹, L. J. Li^{1,64}, Lei Li⁴⁸, M. H. Li⁴³, P. L. Li⁶⁴, P. R. Li^{38,k,l}, Q. M. Li^{1,64},
Q. X. Li⁵⁰, R. Li^{17,31}, T. Li⁵⁰, T. Y. Li⁴³, W. D. Li^{1,64}, W. G. Li^{1,a}, X. Li^{1,64}, X. H. Li^{72,58},
X. L. Li⁵⁰, X. Y. Li^{1,8}, X. Z. Li⁵⁹, Y. Li¹⁹, Y. G. Li^{46,h}, Z. J. Li⁵⁹, Z. Y. Li⁷⁹, C. Liang⁴²,
H. Liang^{72,58}, Y. F. Liang⁵⁴, Y. T. Liang^{31,64}, G. R. Liao¹⁴, Y. P. Liao^{1,64}, J. Libby²⁶, A.
Limphirat⁶⁰, C. C. Lin⁵⁵, C. X. Lin⁶⁴, D. X. Lin^{31,64}, T. Lin¹, B. J. Liu¹, B. X. Liu⁷⁷, C. Liu³⁴,
C. X. Liu¹, F. Liu¹, F. H. Liu⁵³, Feng Liu⁶, G. M. Liu^{56,j}, H. Liu^{38,k,l}, H. B. Liu¹⁵, H. H. Liu¹,
H. M. Liu^{1,64}, Huihui Liu²¹, J. B. Liu^{72,58}, K. Liu^{38,k,l}, K. Y. Liu⁴⁰, Ke Liu²², L. Liu^{72,58},
L. C. Liu⁴³, Lu Liu⁴³, M. H. Liu^{12,g}, P. L. Liu¹, Q. Liu⁶⁴, S. B. Liu^{72,58}, T. Liu^{12,g}, W. K. Liu⁴³,
W. M. Liu^{72,58}, X. Liu^{38,k,l}, X. Liu³⁹, Y. Liu^{38,k,l}, Y. Liu⁸¹, Y. B. Liu⁴³, Z. A. Liu^{1,58,64},
Z. D. Liu⁹, Z. Q. Liu⁵⁰, X. C. Lou^{1,58,64}, F. X. Lu⁵⁹, H. J. Lu²³, J. G. Lu^{1,58}, Y. Lu⁷, Y. P. Lu^{1,58},
Z. H. Lu^{1,64}, C. L. Luo⁴¹, J. R. Luo⁵⁹, M. X. Luo⁸⁰, T. Luo^{12,g}, X. L. Luo^{1,58}, X. R. Lyu⁶⁴,
Y. F. Lyu⁴³, F. C. Ma⁴⁰, H. Ma⁷⁹, H. L. Ma¹, J. L. Ma^{1,64}, L. L. Ma⁵⁰, L. R. Ma⁶⁷, Q. M. Ma¹,
R. Q. Ma^{1,64}, R. Y. Ma¹⁹, T. Ma^{72,58}, X. T. Ma^{1,64}, X. Y. Ma^{1,58}, Y. M. Ma³¹, F. E. Maas¹⁸,

I. MacKay⁷⁰, M. Maggiora^{75A,75C}, S. Malde⁷⁰, Y. J. Mao^{46,h}, Z. P. Mao¹, S. Marcello^{75A,75C},
 Y. H. Meng⁶⁴, Z. X. Meng⁶⁷, J. G. Messchendorp^{13,65}, G. Mezzadri^{29A}, H. Miao^{1,64}, T. J. Min⁴²,
 R. E. Mitchell²⁷, X. H. Mo^{1,58,64}, B. Moses²⁷, N. Yu. Muchnoi^{4,c}, J. Muskalla³⁵, Y. Nefedov³⁶,
 F. Nerling^{18,e}, L. S. Nie²⁰, I. B. Nikolaev^{4,c}, Z. Ning^{1,58}, S. Nisar^{11,m}, Q. L. Niu^{38,k,l},
 W. D. Niu⁵⁵, Y. Niu⁵⁰, S. L. Olsen^{10,64}, Q. Ouyang^{1,58,64}, S. Pacetti^{28B,28C}, X. Pan⁵⁵, Y. Pan⁵⁷,
 A. Pathak¹⁰, Y. P. Pei^{72,58}, M. Pelizaeus³, H. P. Peng^{72,58}, Y. Y. Peng^{38,k,l}, K. Peters^{13,e},
 J. L. Ping⁴¹, R. G. Ping^{1,64}, S. Plura³⁵, V. Prasad³³, F. Z. Qi¹, H. R. Qi⁶¹, M. Qi⁴², S. Qian^{1,58},
 W. B. Qian⁶⁴, C. F. Qiao⁶⁴, J. H. Qiao¹⁹, J. J. Qin⁷³, L. Q. Qin¹⁴, L. Y. Qin^{72,58}, X. P. Qin^{12,g},
 X. S. Qin⁵⁰, Z. H. Qin^{1,58}, J. F. Qiu¹, Z. H. Qu⁷³, C. F. Redmer³⁵, K. J. Ren³⁹, A. Rivetti^{75C},
 M. Rolo^{75C}, G. Rong^{1,64}, Ch. Rosner¹⁸, M. Q. Ruan^{1,58}, S. N. Ruan⁴³, N. Salone⁴⁴,
 A. Sarantsev^{36,d}, Y. Schelhaas³⁵, K. Schoenning⁷⁶, M. Scodreggio^{29A}, K. Y. Shan^{12,g}, W. Shan²⁴,
 X. Y. Shan^{72,58}, Z. J. Shang^{38,k,l}, J. F. Shangguan¹⁶, L. G. Shao^{1,64}, M. Shao^{72,58}, C. P. Shen^{12,g},
 H. F. Shen^{1,8}, W. H. Shen⁶⁴, X. Y. Shen^{1,64}, B. A. Shi⁶⁴, H. Shi^{72,58}, J. L. Shi^{12,g}, J. Y. Shi¹,
 S. Y. Shi⁷³, X. Shi^{1,58}, J. J. Song¹⁹, T. Z. Song⁵⁹, W. M. Song^{34,1}, Y. J. Song^{12,g},
 Y. X. Song^{46,h,n}, S. Sosio^{75A,75C}, S. Spataro^{75A,75C}, F. Stieler³⁵, S. S. Su⁴⁰, Y. J. Su⁶⁴,
 G. B. Sun⁷⁷, G. X. Sun¹, H. Sun⁶⁴, H. K. Sun¹, J. F. Sun¹⁹, K. Sun⁶¹, L. Sun⁷⁷, S. S. Sun^{1,64},
 T. Sun^{51,f}, Y. J. Sun^{72,58}, Y. Z. Sun¹, Z. Q. Sun^{1,64}, Z. T. Sun⁵⁰, C. J. Tang⁵⁴, G. Y. Tang¹,
 J. Tang⁵⁹, M. Tang^{72,58}, Y. A. Tang⁷⁷, L. Y. Tao⁷³, M. Tat⁷⁰, J. X. Teng^{72,58}, V. Thoren⁷⁶,
 W. H. Tian⁵⁹, Y. Tian^{31,64}, Z. F. Tian⁷⁷, I. Uman^{62B}, Y. Wan⁵⁵, S. J. Wang⁵⁰, B. Wang¹,
 Bo Wang^{72,58}, C. Wang¹⁹, D. Y. Wang^{46,h}, H. J. Wang^{38,k,l}, J. J. Wang⁷⁷, J. P. Wang⁵⁰,
 K. Wang^{1,58}, L. L. Wang¹, L. W. Wang³⁴, M. Wang⁵⁰, N. Y. Wang⁶⁴, S. Wang^{38,k,l}, S. Wang^{12,g},
 T. Wang^{12,g}, T. J. Wang⁴³, W. Wang⁵⁹, W. Wang⁷³, W. P. Wang^{35,58,72,o}, X. Wang^{46,h},
 X. F. Wang^{38,k,l}, X. J. Wang³⁹, X. L. Wang^{12,g}, X. N. Wang¹, Y. Wang⁶¹, Y. D. Wang⁴⁵,
 Y. F. Wang^{1,58,64}, Y. H. Wang^{38,k,l}, Y. L. Wang¹⁹, Y. N. Wang⁴⁵, Y. Q. Wang¹, Yaqian Wang¹⁷,
 Yi Wang⁶¹, Z. Wang^{1,58}, Z. L. Wang⁷³, Z. Y. Wang^{1,64}, D. H. Wei¹⁴, F. Weidner⁶⁹, S. P. Wen¹,
 Y. R. Wen³⁹, U. Wiedner³, G. Wilkinson⁷⁰, M. Wolke⁷⁶, L. Wollenberg³, C. Wu³⁹, J. F. Wu^{1,8},
 L. H. Wu¹, L. J. Wu^{1,64}, Lianjie Wu¹⁹, X. Wu^{12,g}, X. H. Wu³⁴, Y. H. Wu⁵⁵, Y. J. Wu³¹,
 Z. Wu^{1,58}, L. Xia^{72,58}, X. M. Xian³⁹, B. H. Xiang^{1,64}, T. Xiang^{46,h}, D. Xiao^{38,k,l}, G. Y. Xiao⁴²,
 H. Xiao⁷³, Y. L. Xiao^{12,g}, Z. J. Xiao⁴¹, C. Xie⁴², X. H. Xie^{46,h}, Y. Xie⁵⁰, Y. G. Xie^{1,58},
 Y. H. Xie⁶, Z. P. Xie^{72,58}, T. Y. Xing^{1,64}, C. F. Xu^{1,64}, C. J. Xu⁵⁹, G. F. Xu¹, M. Xu^{72,58},
 Q. J. Xu¹⁶, Q. N. Xu³⁰, W. L. Xu⁶⁷, X. P. Xu⁵⁵, Y. Xu⁴⁰, Y. C. Xu⁷⁸, Z. S. Xu⁶⁴, F. Yan^{12,g},
 L. Yan^{12,g}, W. B. Yan^{72,58}, W. C. Yan⁸¹, W. P. Yan¹⁹, X. Q. Yan^{1,64}, H. J. Yang^{51,f},
 H. L. Yang³⁴, H. X. Yang¹, J. H. Yang⁴², R. J. Yang¹⁹, T. Yang¹, Y. Yang^{12,g}, Y. F. Yang⁴³,
 Y. X. Yang^{1,64}, Y. Z. Yang¹⁹, Z. W. Yang^{38,k,l}, Z. P. Yao⁵⁰, M. Ye^{1,58}, M. H. Ye⁸, Junhao Yin⁴³,
 Z. Y. You⁵⁹, B. X. Yu^{1,58,64}, C. X. Yu⁴³, G. Yu¹³, J. S. Yu^{25,i}, M. C. Yu⁴⁰, T. Yu⁷³, X. D. Yu^{46,h},
 C. Z. Yuan^{1,64}, J. Yuan³⁴, J. Yuan⁴⁵, L. Yuan², S. C. Yuan^{1,64}, Y. Yuan^{1,64}, Z. Y. Yuan⁵⁹,
 C. X. Yue³⁹, Ying Yue¹⁹, A. A. Zafar⁷⁴, F. R. Zeng⁵⁰, S. H. Zeng^{63A,63B,63C,63D}, X. Zeng^{12,g},
 Y. Zeng^{25,i}, Y. J. Zeng⁵⁹, Y. J. Zeng^{1,64}, X. Y. Zhai³⁴, Y. C. Zhai⁵⁰, Y. H. Zhan⁵⁹,
 A. Q. Zhang^{1,64}, B. L. Zhang^{1,64}, B. X. Zhang¹, D. H. Zhang⁴³, G. Y. Zhang¹⁹, H. Zhang^{72,58},
 H. Zhang⁸¹, H. C. Zhang^{1,58,64}, H. H. Zhang⁵⁹, H. Q. Zhang^{1,58,64}, H. R. Zhang^{72,58},
 H. Y. Zhang^{1,58}, J. Zhang⁵⁹, J. Zhang⁸¹, J. J. Zhang⁵², J. L. Zhang²⁰, J. Q. Zhang⁴¹,
 J. S. Zhang^{12,g}, J. W. Zhang^{1,58,64}, J. X. Zhang^{38,k,l}, J. Y. Zhang¹, J. Z. Zhang^{1,64},
 Jianyu Zhang⁶⁴, L. M. Zhang⁶¹, Lei Zhang⁴², P. Zhang^{1,64}, Q. Zhang¹⁹, Q. Y. Zhang³⁴,
 R. Y. Zhang^{38,k,l}, S. H. Zhang^{1,64}, Shulei Zhang^{25,i}, X. M. Zhang¹, X. Y. Zhang⁴⁰, X. Y. Zhang⁵⁰,
 Y. Zhang¹, Y. Zhang⁷³, Y. T. Zhang⁸¹, Y. H. Zhang^{1,58}, Y. M. Zhang³⁹, Yan Zhang^{72,58},
 Z. D. Zhang¹, Z. H. Zhang¹, Z. L. Zhang³⁴, Z. X. Zhang¹⁹, Z. Y. Zhang⁴³, Z. Y. Zhang⁷⁷, Z. Z.
 Zhang⁴⁵, Zh. Zh. Zhang¹⁹, G. Zhao¹, J. Y. Zhao^{1,64}, J. Z. Zhao^{1,58}, L. Zhao¹, Lei Zhao^{72,58},
 M. G. Zhao⁴³, N. Zhao⁷⁹, R. P. Zhao⁶⁴, S. J. Zhao⁸¹, Y. B. Zhao^{1,58}, Y. X. Zhao^{31,64},

Z. G. Zhao^{72,58}, A. Zhemchugov^{36,b}, B. Zheng⁷³, B. M. Zheng³⁴, J. P. Zheng^{1,58}, W. J. Zheng^{1,64}, X. R. Zheng¹⁹, Y. H. Zheng⁶⁴, B. Zhong⁴¹, X. Zhong⁵⁹, H. Zhou^{35,50,o}, J. Y. Zhou³⁴, S. Zhou⁶, X. Zhou⁷⁷, X. K. Zhou⁶, X. R. Zhou^{72,58}, X. Y. Zhou³⁹, Y. Z. Zhou^{12,g}, Z. C. Zhou²⁰, A. N. Zhu⁶⁴, J. Zhu⁴³, K. Zhu¹, K. J. Zhu^{1,58,64}, K. S. Zhu^{12,g}, L. Zhu³⁴, L. X. Zhu⁶⁴, S. H. Zhu⁷¹, T. J. Zhu^{12,g}, W. D. Zhu⁴¹, W. J. Zhu¹, W. Z. Zhu¹⁹, Y. C. Zhu^{72,58}, Z. A. Zhu^{1,64}, J. H. Zou¹, J. Zu^{72,58}

(BESIII Collaboration)

¹ *Institute of High Energy Physics, Beijing 100049, People's Republic of China*

² *Beihang University, Beijing 100191, People's Republic of China*

³ *Bochum Ruhr-University, D-44780 Bochum, Germany*

⁴ *Budker Institute of Nuclear Physics SB RAS (BINP), Novosibirsk 630090, Russia*

⁵ *Carnegie Mellon University, Pittsburgh, Pennsylvania 15213, USA*

⁶ *Central China Normal University, Wuhan 430079, People's Republic of China*

⁷ *Central South University, Changsha 410083, People's Republic of China*

⁸ *China Center of Advanced Science and Technology, Beijing 100190, People's Republic of China*

⁹ *China University of Geosciences, Wuhan 430074, People's Republic of China*

¹⁰ *Chung-Ang University, Seoul, 06974, Republic of Korea*

¹¹ *COMSATS University Islamabad, Lahore Campus, Defence Road, Off Raiwind Road, 54000 Lahore, Pakistan*

¹² *Fudan University, Shanghai 200433, People's Republic of China*

¹³ *GSI Helmholtzcentre for Heavy Ion Research GmbH, D-64291 Darmstadt, Germany*

¹⁴ *Guangxi Normal University, Guilin 541004, People's Republic of China*

¹⁵ *Guangxi University, Nanning 530004, People's Republic of China*

¹⁶ *Hangzhou Normal University, Hangzhou 310036, People's Republic of China*

¹⁷ *Hebei University, Baoding 071002, People's Republic of China*

¹⁸ *Helmholtz Institute Mainz, Staudinger Weg 18, D-55099 Mainz, Germany*

¹⁹ *Henan Normal University, Xinxiang 453007, People's Republic of China*

²⁰ *Henan University, Kaifeng 475004, People's Republic of China*

²¹ *Henan University of Science and Technology, Luoyang 471003, People's Republic of China*

²² *Henan University of Technology, Zhengzhou 450001, People's Republic of China*

²³ *Huangshan College, Huangshan 245000, People's Republic of China*

²⁴ *Hunan Normal University, Changsha 410081, People's Republic of China*

²⁵ *Hunan University, Changsha 410082, People's Republic of China*

²⁶ *Indian Institute of Technology Madras, Chennai 600036, India*

²⁷ *Indiana University, Bloomington, Indiana 47405, USA*

²⁸ *INFN Laboratori Nazionali di Frascati, (A)INFN Laboratori Nazionali di Frascati, I-00044, Frascati, Italy; (B)INFN Sezione di Perugia, I-06100, Perugia, Italy; (C)University of Perugia, I-06100, Perugia, Italy*

²⁹ *INFN Sezione di Ferrara, (A)INFN Sezione di Ferrara, I-44122, Ferrara, Italy; (B)University of Ferrara, I-44122, Ferrara, Italy*

³⁰ *Inner Mongolia University, Hohhot 010021, People's Republic of China*

³¹ *Institute of Modern Physics, Lanzhou 730000, People's Republic of China*

³² *Institute of Physics and Technology, Peace Avenue 54B, Ulaanbaatar 13330, Mongolia*

³³ *Instituto de Alta Investigación, Universidad de Tarapacá, Casilla 7D, Arica 1000000, Chile*

³⁴ *Jilin University, Changchun 130012, People's Republic of China*

³⁵ *Johannes Gutenberg University of Mainz, Johann-Joachim-Becher-Weg 45, D-55099 Mainz, Germany*

- ³⁶ *Joint Institute for Nuclear Research, 141980 Dubna, Moscow region, Russia*
- ³⁷ *Justus-Liebig-Universitaet Giessen, II. Physikalisches Institut, Heinrich-Buff-Ring 16, D-35392 Giessen, Germany*
- ³⁸ *Lanzhou University, Lanzhou 730000, People's Republic of China*
- ³⁹ *Liaoning Normal University, Dalian 116029, People's Republic of China*
- ⁴⁰ *Liaoning University, Shenyang 110036, People's Republic of China*
- ⁴¹ *Nanjing Normal University, Nanjing 210023, People's Republic of China*
- ⁴² *Nanjing University, Nanjing 210093, People's Republic of China*
- ⁴³ *Nankai University, Tianjin 300071, People's Republic of China*
- ⁴⁴ *National Centre for Nuclear Research, Warsaw 02-093, Poland*
- ⁴⁵ *North China Electric Power University, Beijing 102206, People's Republic of China*
- ⁴⁶ *Peking University, Beijing 100871, People's Republic of China*
- ⁴⁷ *Qufu Normal University, Qufu 273165, People's Republic of China*
- ⁴⁸ *Renmin University of China, Beijing 100872, People's Republic of China*
- ⁴⁹ *Shandong Normal University, Jinan 250014, People's Republic of China*
- ⁵⁰ *Shandong University, Jinan 250100, People's Republic of China*
- ⁵¹ *Shanghai Jiao Tong University, Shanghai 200240, People's Republic of China*
- ⁵² *Shanxi Normal University, Linfen 041004, People's Republic of China*
- ⁵³ *Shanxi University, Taiyuan 030006, People's Republic of China*
- ⁵⁴ *Sichuan University, Chengdu 610064, People's Republic of China*
- ⁵⁵ *Soochow University, Suzhou 215006, People's Republic of China*
- ⁵⁶ *South China Normal University, Guangzhou 510006, People's Republic of China*
- ⁵⁷ *Southeast University, Nanjing 211100, People's Republic of China*
- ⁵⁸ *State Key Laboratory of Particle Detection and Electronics, Beijing 100049, Hefei 230026, People's Republic of China*
- ⁵⁹ *Sun Yat-Sen University, Guangzhou 510275, People's Republic of China*
- ⁶⁰ *Suranaree University of Technology, University Avenue 111, Nakhon Ratchasima 30000, Thailand*
- ⁶¹ *Tsinghua University, Beijing 100084, People's Republic of China*
- ⁶² *Turkish Accelerator Center Particle Factory Group, (A)Istinye University, 34010, Istanbul, Turkey; (B)Near East University, Nicosia, North Cyprus, 99138, Mersin 10, Turkey*
- ⁶³ *University of Bristol, H H Wills Physics Laboratory, Tyndall Avenue, Bristol, BS8 1TL, UK*
- ⁶⁴ *University of Chinese Academy of Sciences, Beijing 100049, People's Republic of China*
- ⁶⁵ *University of Groningen, NL-9747 AA Groningen, The Netherlands*
- ⁶⁶ *University of Hawaii, Honolulu, Hawaii 96822, USA*
- ⁶⁷ *University of Jinan, Jinan 250022, People's Republic of China*
- ⁶⁸ *University of Manchester, Oxford Road, Manchester, M13 9PL, United Kingdom*
- ⁶⁹ *University of Muenster, Wilhelm-Klemm-Strasse 9, 48149 Muenster, Germany*
- ⁷⁰ *University of Oxford, Keble Road, Oxford OX13RH, United Kingdom*
- ⁷¹ *University of Science and Technology Liaoning, Anshan 114051, People's Republic of China*
- ⁷² *University of Science and Technology of China, Hefei 230026, People's Republic of China*
- ⁷³ *University of South China, Hengyang 421001, People's Republic of China*
- ⁷⁴ *University of the Punjab, Lahore-54590, Pakistan*
- ⁷⁵ *University of Turin and INFN, (A)University of Turin, I-10125, Turin, Italy; (B)University of Eastern Piedmont, I-15121, Alessandria, Italy; (C)INFN, I-10125, Turin, Italy*
- ⁷⁶ *Uppsala University, Box 516, SE-75120 Uppsala, Sweden*
- ⁷⁷ *Wuhan University, Wuhan 430072, People's Republic of China*
- ⁷⁸ *Yantai University, Yantai 264005, People's Republic of China*

⁷⁹ *Yunnan University, Kunming 650500, People's Republic of China*

⁸⁰ *Zhejiang University, Hangzhou 310027, People's Republic of China*

⁸¹ *Zhengzhou University, Zhengzhou 450001, People's Republic of China*

^a *Deceased*

^b *Also at the Moscow Institute of Physics and Technology, Moscow 141700, Russia*

^c *Also at the Novosibirsk State University, Novosibirsk, 630090, Russia*

^d *Also at the NRC "Kurchatov Institute", PNPI, 188300, Gatchina, Russia*

^e *Also at Goethe University Frankfurt, 60323 Frankfurt am Main, Germany*

^f *Also at Key Laboratory for Particle Physics, Astrophysics and Cosmology, Ministry of Education; Shanghai Key Laboratory for Particle Physics and Cosmology; Institute of Nuclear and Particle Physics, Shanghai 200240, People's Republic of China*

^g *Also at Key Laboratory of Nuclear Physics and Ion-beam Application (MOE) and Institute of Modern Physics, Fudan University, Shanghai 200443, People's Republic of China*

^h *Also at State Key Laboratory of Nuclear Physics and Technology, Peking University, Beijing 100871, People's Republic of China*

ⁱ *Also at School of Physics and Electronics, Hunan University, Changsha 410082, China*

^j *Also at Guangdong Provincial Key Laboratory of Nuclear Science, Institute of Quantum Matter, South China Normal University, Guangzhou 510006, China*

^k *Also at MOE Frontiers Science Center for Rare Isotopes, Lanzhou University, Lanzhou 730000, People's Republic of China*

^l *Also at Lanzhou Center for Theoretical Physics, Lanzhou University, Lanzhou 730000, People's Republic of China*

^m *Also at the Department of Mathematical Sciences, IBA, Karachi 75270, Pakistan*

ⁿ *Also at Ecole Polytechnique Federale de Lausanne (EPFL), CH-1015 Lausanne, Switzerland*

^o *Also at Helmholtz Institute Mainz, Staudinger Weg 18, D-55099 Mainz, Germany*